Accepted Manuscript

New $Li_3Ni_2NbO_6$ microwave dielectric ceramics with the orthorhombic structure for LTCC applications

H.L. Pan, Y.X. Mao, L. Cheng, H.T. Wu

PII: S0925-8388(17)32293-4

DOI: 10.1016/j.jallcom.2017.06.285

Reference: JALCOM 42354

To appear in: *Journal of Alloys and Compounds*

Received Date: 8 December 2016

Revised Date: 15 June 2017

Accepted Date: 25 June 2017

Please cite this article as: H.L. Pan, Y.X. Mao, L. Cheng, H.T. Wu, New $Li_3Ni_2NbO_6$ microwave dielectric ceramics with the orthorhombic structure for LTCC applications, *Journal of Alloys and Compounds* (2017), doi: 10.1016/j.jallcom.2017.06.285.

Graphical Abstract

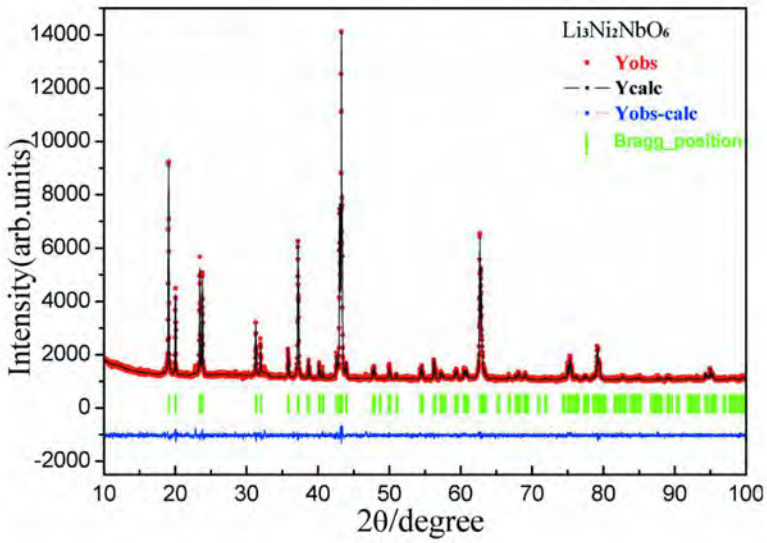

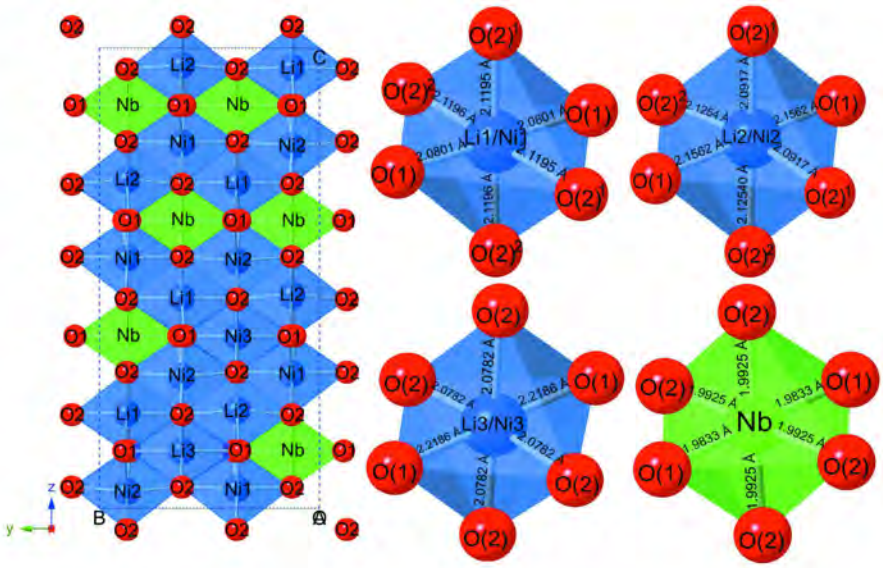

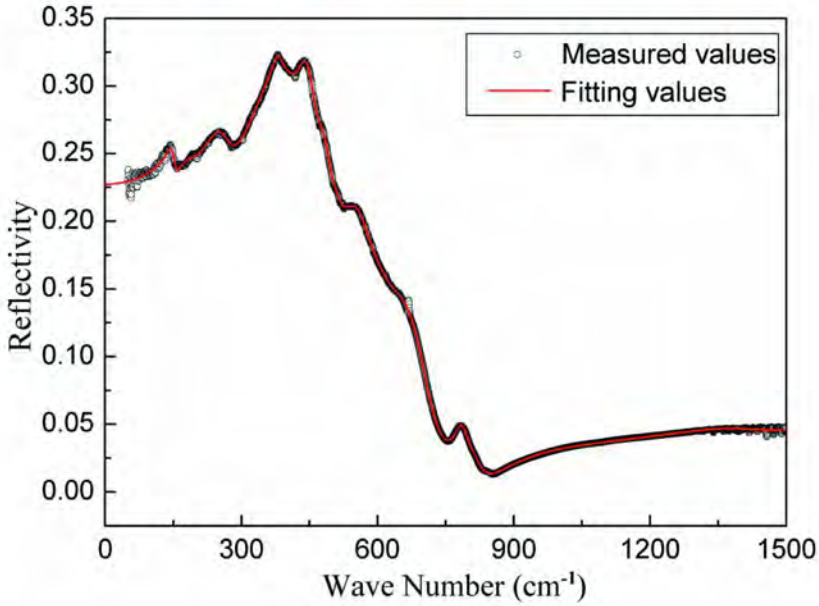

New $Li_3Ni_2NbO_6$ microwave dielectric ceramics with the orthorhombic structure for LTCC applications

H.L. Pan, Y.X. Mao, L. Cheng, H.T. Wu*

School of Materials Science and Engineering, University of Jinan, Jinan 250022, China

Abstract: New $Li_3Ni_2NbO_6$ (indexed as LNN) microwave dielectric ceramics were prepared by the conventional solid-state method. The phase composition, crystal structure, sintering characteristics, micro-structures, microwave dielectric properties, intrinsic factors and vibrational phonon modes were investigated. XRD results showed that LNN phase exhibit orthorhombic structure with Fddd (No. 70) space group. Rietveld refinement was applied to analyze the crystalline structure and the lattice parameters were obtained. On the basis of the chemical bond theory and lattice parameters, the bond ionicity, lattice energy, bond energy and coefficient of thermal expansion were calculated to evaluate the structural characteristics. Nb-O bonds played an important role in affecting the microwave dielectric proprieties of LNN ceramics. The results of Infrared reflectivity spectrum indicated that the absorptions of phonon oscillation played an important influence on the dielectric contribution of LNN ceramics. At the sintering temperature of 850 °C, excellent microwave dielectric properties of ε_r=15.85, $Q \cdot f$=19,860 GHz and τ_f=-15.45 ppm/°C were obtained for LNN ceramics. The excellent microwave dielectric properties and low sintering temperature of LNN ceramics made it a promising candidate for low temperature co-fired ceramics (indexed as LTCC) applications.

Keywords: LTCC; $Li_3Ni_2NbO_6$; Microwave dielectric properties; Chemical bond theory

*Corresponding author.
Tel.: +86 531 82765473; fax: +86 531 87974453.
E-mail address: mse_wuht@ujn.edu.cn (H.T. Wu)

1. Introduction

With the rapid development of satellite communication and wireless communications systems, the low temperature co-fired ceramics technology has obtained much attentions due to its advantage and simplicity in integrating and minimizing electronic components [1, 2]. LTCC should meet some requirements: a low sintering temperature (below melting points of Ag, Cu, etc.), a high quality factor, an appropriate dielectric permittivity, a near-zero temperature coefficient of resonant frequency and a good chemical compatibility [3, 4]. Even though many microwave ceramics with good dielectric properties are commercially available, they are not suitable for LTCC applications owing to their high sintering temperatures [5, 6]. How to decrease the sintering temperature is a key issue in applying this technology. Generally speaking, there are several techniques to lower the sintering temperature, such as using the wet chemistry route [7, 8], searching for novel glass-free low-sintering dielectric ceramics [9] and adding low melting temperature sintering aids [10]. The wet chemistry route often is complex and time consuming. Low melting temperature sintering aids are added to the ceramics systems to effectively reduce the sintering temperature, but this in turn deteriorates the microwave dielectric properties, especially the quality factor [2, 10]. Therefore, new microwave dielectric ceramics with intrinsically low sintering temperatures have to be developed.

Recently, many compounds based on Li_2O-AO-B_2O_5 (A=Mg, Zn, Ni and B=Nb, Ta, Sb) systems were reported for the possible used in microwave communications [11-14]. For example, Yuan et al. [11] reported that $Li_3Mg_2NbO_6$ ceramics sintered at 1250 °C exhibited the microwave dielectric properties of ε_r=16.80, $Q\cdot f$=79,643 GHz and τ_f=-27.20 ppm/°C, and $Li_3Zn_2SbO_6$ ceramics exhibited the microwave dielectric properties of ε_r=10.50, $Q\cdot f$=56,000 GHz and τ_f=-25.60 ppm/°C at 1450 °C, respectively. In our previous work, the correlations between the structure and microwave dielectric

properties of $Li_3Mg_2NbO_6$ were researched and microwave dielectric properties of ε_r=14.94, $Q \cdot f$=100,965 GHz, and τ_f=-21.96 ppm/°C were also reported [12]. Until now, a few literature on LNN phase have been reported. For instance, the preparation and crystal structure of LNN phase were reported by Mather et al. for the first time [15]. Subsequently, West et al. [16] investigated the continuous order-disorder transition for LNN phase and the rock salt structures of Cr-doped LNN. Not long ago, Kawasoko et al. [17] reported the self-assembly of LNN epitaxial disks with very low height/width aspect ratios. However, to the best of our knowledge, the microwave dielectric properties of LNN ceramics have not been reported. In this work, firstly, LNN ceramics were prepared by the solid-state method. Subsequently, the crystal structure, sintering characteristics and micro-structures were also researched. Moreover, the correlations between microwave dielectric properties and sintering temperatures were discussed systematically. Finally, the bond ionicity, lattice energy, coefficient of thermal expansion and bond energy were calculated to evaluate the structural characteristics and Infrared reflectivity spectrum was also investigated.

2. Experimental procedure

LNN ceramics were prepared by the conventional solid-state method. High-purity Li_2CO_3 (99.99%, Aladdin), NiO (99.9%, Aladdin) and Nb_2O_5 (99.99%, Aladdin) were weighed and mixed according to the chemical formula of LNN. The mixed powders were ball-milled in a nylon container for 8 h and then calcined at 700 °C for 4 h. The calcined powders with paraffin wax were pressed into pellets of 10 mm in diameter and 5 mm in thickness at a pressure of 200 MPa. These pellets were preheated at 500 °C to expel the binder and then sintered at 750-950 °C for 4 h in air at a heating rate of 5 °C/min. The sintered samples were not performed any standard surface preparation (polishing, etching, etc.).

The crystalline phase was identified by X-ray diffraction (Model D/MAX-B, Rigaku Co., Japan) with CuKα radiation (λ=0.1542 nm) attached with the monochromator. Scanning electron microscopy (Model JEOL JEM-2010, FEI Co., Japan) was utilized to observe the surface morphology. Rietveld refinement was performed using Fullprof program. The reliability of the refinement results was judged by the pattern R factor (R_p), weighted pattern R factor (R_{wp}) and goodness of fit indicator (χ^2). The infrared reflectivity spectra were measured using a Bruker IFS 66v Fourier transform infrared (FTIR) spectrometer on Infrared beamline station (U4) at National Synchrotron Radiation Lab., China. A network analyzer (N5234A, Agilent Co., America) was used to measure the microwave dielectric properties. ε_r value was measured by Hakki-Coleman method [18] and $Q \cdot f$ was measured by cavity method [19]. τ_f was measured at the temperatures of 25-85 °C and calculated by the following formula.

$$\tau_f = \frac{f_2 - f_1}{f_1(T_2 - T_1)} \tag{1}$$

where f_1 and f_2 were the resonant frequency at T_1 (25 °C) and T_2 (85 °C), respectively.

The apparent density of the samples was measured using Archimedes method (Mettler Toledo XS64). To obtain the relative density of the samples, the theoretical density was calculated through the cell parameters and the atomic weight [20] using Equ. (2).

$$\rho_{\text{theory}} = \frac{ZA}{V_C N_A} \tag{2}$$

where Z, A, V_C and N_A are the number of atoms in the unit cell, all the atomic weights in the unit cell, volume of the unit cell and Avogadro constant, respectively. The relative density was obtained using Equ. (3).

$$\rho_{\text{relative}} = \frac{\rho_{\text{apparent}}}{\rho_{\text{theory}}} \times 100\,\% \tag{3}$$

3. Results and discussion

Fig. 1 shows X-ray diffraction patterns of LNN samples sintered at 750-950 °C. The predominant phase is identified as the orthorhombic structure LNN phase (JCPDS No. 48-0324) with Fddd (No. 70) space group while just a minor unknown phases are detected. With the increase of the sintering temperatures from 750 °C to 950 °C, there is no significant change for the XRD patterns. As can be seen from the enlarged drawing, the peak positions show no apparent deviation, which indicates no change of the cell volume.

A typical pattern plot of the LNN sample sintered at 850 °C after refinement all of the parameters is illustrated in Fig. 2. The LNN phase reported by West et al. [16], was adopted as the starting model. The calculated pattern is overlaid on the measured pattern and the differences between two profiles were plotted along the bottom. It is found that the measured pattern fits well with the calculated pattern. The quality of the refinement are R_p=2.56 %, R_{wp}=3.26 % and χ^2=1.4. The refinement parameters such as the cell parameters, atomic positions and occupations are given in Table 1. The lattice parameters are calculated to be a =5.9066 Å, b=8.4039 Å, c=17.7444 Å, α=β=γ=90° and V_m=880.7927 $Å^3$, which are employed to calculate the bond length of cation-oxygen bonds as shown in Table 2.

The schematic representation of the crystal structure is shown in Fig. 3. It can be seen that LNN is constituted by the A-site (A=Li^+, Ni^{2+}) and B-site (B=Nb^{5+}) oxygen octahedrons. Li^+/Ni^{2+} and Nb^{5+} cations are octahedrally connected to four O(2) and two O(1), individually. In this structure, Li1/Ni1 and Li2/Ni2 cations occupy the 16g Wyckoff position. Li3/Ni3 and Nb cations occupy the 8b and 8a Wyckoff positions, respectively. O(1) and O(2) anions occupy the 16f and 32h Wyckoff positions, respectively.

Fig. 4 illustrates the curves of the diametric shrinking ratio, apparent density and relative density of LNN samples as a function of sintering temperatures, which can be used to determine the optimal

sintering temperature. With the increase of the sintering temperatures from 750 °C to 950 °C, these three curves show the similar tendency. For example, the apparent density initially increase and then decrease after reaching a maximum value of 4.8283 g/cm^3 at 850 °C. At the sintering temperature of 850 °C, the relative density reaches 97.84%. The results indicate that the nearly full density could be obtained at 850 °C.

SEM micrographs of LNN ceramics sintered at 750-950 °C are shown in Fig. 5. A small amount of impurity particles can be found in Fig. 5 (a-e), which corresponds to the results that just a minor unknown phases are detected in Fig. 1. With the increase of the sintering temperatures from 750 °C to 950 °C, the average grain size increases from 1.2549 μm to 5.818 μm [21] and the porosity gradually reduce. At the sintering temperature of 850 °C shown in Fig. 5(c), all pores almost disappear on the surface. The increase of the average grain size and the decrease of the pores can explain the increase of the shrinkage ratio and apparent density. At the sintering temperatures of 900 °C and 950 °C, the phenomenon of abnormal grain growth begins to appear due to the excessive temperatures, which can explain the decrease of the shrinkage ratio and apparent density shown in Fig. 4. These phenomena may bring about the harmful influence to the microwave dielectric properties.

Fig. 5 (f) indicates EDS analysis of grains chosen from the samples sintered at 850 °C. Li element can not been detected due to the absorption of X ray on Li element by Be window. C element can be detected because C element is splashed to the specimen surface to increase the conductivity. Point is chosen from the grain and the concentrations of Ni, Nb and O ions are analyzed to be 24.71, 12.66 and 62.63 at%, respectively. The ratio of Ni/Nb/O is approximately corresponding to the formula of LNN phase.

Changes of ε_r, $Q{\cdot}f$ and τ_f values of LNN samples as a function of the sintering temperature are given in Fig. 6. It has been reported that the ε_r value is dependent on the density, dielectric polarizabilities, distortion and rattling of oxygen octahedron [9, 12]. In this work, the ε_r values initially increase and then decrease as the sintering temperatures increase from 750 °C to 950 °C. The increase can be explained by the reduction of the porosity. The decrease can be attributed to the abnormal grain growth and reduction of the density. The variation trend of ε_r is similar to that of the apparent density and diametric shrinking ratio.

To explain the influence of the crystal structure on ε_r, the theoretical dielectric polarizability ($\alpha_{theo.}$) is calculated to be 22.09 on the basis of the additive rule as shown in Equ. (4) [22] and the observed dielectric polarizability ($\alpha_{obs.}$) of the LNN ceramics sintered at 850 °C is calculated to be 21.86 using Clausius-Mossotti equation as formulated in Equ. (5) [23]. The $\alpha_{obs.}$ approximately equal to $\alpha_{theo.}$ and the minor deviation can be explained by the reason that $\alpha_{obs.}$ is easily affected by the fabrication process.

$$\alpha_{theo.}(Li_3Ni_2NbO_6) = 3\alpha(Li^+) + 2\alpha(Ni^{2+}) + \alpha(Nb^{5+}) + 6\alpha(O^{2-}) \quad (4)$$

$$\alpha_{obs.} = \frac{1}{b}V_m\frac{\varepsilon - 1}{\varepsilon + 2} \quad (5)$$

Where $\alpha\ (Li^+)$=1.20 Å^3, $\alpha\ (Ni^{2+})$=1.23 Å^3, $\alpha\ (O^{2-})$=2.01 Å^3, and $\alpha\ (Nb^{5+})$=3.97 Å^3 were reported by Shannon [23]. Moreover, V_m, ε and b indicates the molar volume, dielectric constant and constant value ($4\pi/3$), respectively.

The $Q{\cdot}f$ values are affected by extrinsic factors such as second phases, densification and porosity, and intrinsic factors such as lattice vibration modes, lattice defects, etc. [9, 12]. In our work, $Q{\cdot}f$ values increase to a maximum value and thereafter slightly decrease with the increase of the sintering temperatures from 750 °C to 950 °C. The remarkable increase is interpreted by the growth of grains

according to SEM micro-structures in Fig. 5 (a-c), and the slightly decrease of the $Q \cdot f$ values can be attributed to the abnormal grain growth in Fig. 5 (d-e). Fig. 5 also exhibits the τ_f variation of LNN ceramics as a function of the sintering temperature. τ_f values change from -8.12 to -16.21 ppm/°C during the temperatures of 750-950 °C.

It is reported that microwave properties are dependent on extrinsic factors such as the density, impurity and secondary phase, and intrinsic factors such as the crystal structure and lattice defects [9, 12]. The intrinsic parameters of LNN are further characterized using the chemical bond theory. Many binary crystals such as A^NB^{8-N} could be dealt with using the PV theory [24-26]. Levine [27, 28] successfully solved the complex crystals such as ABC_2, ABC_3, ABC_4. However, an accurate expression was not given for decomposing the complex crystals into the binary crystals. After considering these problems in chemical bond representation, Zhang et al. [29-31] succeed in generalizing the P-V-L theory for multibond systems and gave an explicit expression for decomposing the complex crystals into binary crystals. On the basis of the chemical bond theory and lattice parameters, the complex crystals LNN could be firstly decomposed into the binary crystals as shown in Eq. (6).

$$\begin{aligned} LNN=&Li_{(1)}Li_{(2)}Li_{(3)}2/3Ni_{(1)}2/3Ni_{(2)}2/3Ni_{(3)}2NbO_{(1)}4O_{(2)} \\ =&2/3(Li_{(1)}Ni_{(1)})2/3O_{(1)}+4/3(Li_{(1)}Ni_{(1)})4/3O_{(2)} \\ &+2/3(Li_{(2)}Ni_{(2)})2/3O_{(1)}+4/3(Li_{(2)}Ni_{(2)})4/3O_{(2)} \\ &+1/3(Li_{(3)}Ni_{(3)})1/3O_{(1)}+2/3(Li_{(3)}Ni_{(3)})2/3O_{(2)} \\ &+1/3Nb1/3O_{(1)}+2/3Nb2/3O_{(2)} \end{aligned} \quad (6)$$

It is well known that the concept of the chemical bond ionicity is very important for explaining many basic properties in diverse area [32-34]. The chemical bond ionicity can be evaluated by the generalized P-V-L theory [29-31]. According to the generalized P-V-L theory , the bond ionicity of an

individual bond can be calculated as follows.

$$f_i = \frac{(C^\mu)^2}{(E_g^\mu)^2} \tag{7}$$

$$(E_g^\mu)^2 = (E_h^\mu)^2 + (C^\mu)^2 \tag{8}$$

$$(E_h^\mu)^2 = \frac{39.74}{(d^\mu)^{2.48}} \tag{9}$$

$$C^\mu = 14.4 b^\mu \exp(-k_s^u r_0^\mu)[(Z_A^u)^* - \frac{n}{m}(Z_B^u)^*] / r_0^\mu \tag{10}$$

Where E_g^μ is the average energy gap for the bond μ and it can be decomposed into the homopolar E_h^μ and heteropolar C^μ parts. Some parameters such as $\exp(-k_s^u r_0^\mu)$ and b^μ in Equ. 10 can be obtained from reference [35]. The calculated results of the bond ionicity are listed in Table 3. On the basis of the results of the average bond ionicity $Af_{i(Ni\text{-}O)}<Af_{i(Li\text{-}O)}<Af_{i(Nb\text{-}O)}$, the bond ionicity $f_{i(Nb\text{-}O)}$ makes predominant contribution to the dielectric constant in LNN ceramics. In our previous report, the average bond ionicity of Nb-O bonds was 0.9872 and the dielectric constant was 14.94 for $Li_3Mg_2NbO_6$ ceramics [12]. In this paper, the average bond ionicity of Nb-O bonds is 0.9874 and the dielectric constant is 15.85 for LNN ceramics. The dielectric constant shows the positive correlation with the bond ionicity of Nb-O bonds for $Li_3Mg_2NbO_6$ and $Li_3Ni_2NbO_6$ ceramics.

As for the lattice energy, the parameters of a single bond could also be separated into the ionic and covalent parts. On the basis of the generalized P-V-L theory [29-31], the lattice energy U of the LNN crystal is calculated by Equs. (11-14).

$$U = \sum_\mu U_b^\mu \tag{11}$$

$$U_b^\mu = U_{bc}^\mu + U_{bi}^\mu \tag{12}$$

$$U_{bc}^\mu = 2100 m \frac{(Z_+^\mu)^{1.64}}{(d^\mu)^{0.75}} f_C^\mu \tag{13}$$

$$U_{bi}^\mu = 1270 \frac{(m+n) Z_+^\mu Z_-^\mu}{d^\mu}(1 - \frac{0.4}{d^\mu}) f_i^\mu \tag{14}$$

Where U_{bc}^{μ} is the covalent part and U_{bi}^{μ} is the ionic part of μ bond. Z_{+}^{μ} and Z_{-}^{μ} are the valence states of the cation and anion, respectively. The calculated results of the lattice energies are listed in Table 3. Obviously, According to results of the average lattice energy $AU_{(Ni\text{-}O)}<AU_{(Li\text{-}O)}<AU_{(Nb\text{-}O)}$, the lattice energy $U_{(Nb\text{-}O)}$ plays major role in affecting $Q{\cdot}f$ value as intrinsic factors in LNN ceramics. In our previous report, the average lattice energy of Nb-O bonds was 12750 KJ/mol and the quality factor was 100,965 GHz for $Li_3Mg_2NbO_6$ ceramics [12]. In this paper, the average lattice energy of Nb-O bonds is 12670 KJ/mol and the quality factor is 1,9860 GHz for LNN ceramics. The quality factor shows the positive correlation with the lattice energy of Nb-O bonds for $Li_3Mg_2NbO_6$ and $Li_3Ni_2NbO_6$ ceramics.

On the basis of the chemical bond theory and crystal parameter, the coefficient of thermal expansion α can be written as the following Equ. (15).

$$\alpha = \sum_{\mu} F_{mn}^{\mu} \alpha_{mn}^{\mu} \tag{15}$$

Where F_{mn}^{μ} is the proportion of μ bond in the total bonds. For any binary compounds A_mB_n, the coefficient of thermal expansion α_{mn}^{μ} can be calculated as the following Eqs. (16-18).

$$\alpha_{mn}^{\mu} = -3.1685 + 0.8376\ \gamma_{mn} \tag{16}$$

$$\gamma_{mn} = \frac{kZ_{A}^{\mu} N_{CA}^{\mu}}{U_{b}^{\mu}\ \Delta_{A}} \beta_{mn} \tag{17}$$

$$\beta_{mn} = \frac{m(m+n)}{2n} \tag{18}$$

Where k is Boltzmann constant, Z_{A}^{μ} is the valence states of cation, N_{CA}^{μ} is the coordination number of μ bond for cation A. The calculated results of the coefficient of the thermal expansion are listed in Table 3. According to the results, the Nb-O bonds exhibits the stable coefficient of thermal expansion. Based on the results of the average coefficient of thermal expansion $A\alpha_{(Nb\text{-}O)}<A\alpha_{(Ni\text{-}O)}<A\alpha_{(Li\text{-}O)}$, the temperature coefficient of resonant frequency τ_f would mainly be affected by the coefficient of the

thermal expansion of Nb-O bonds. It is suggested that the α value is also a key factor influencing the temperature coefficient of resonant frequency of LNN ceramics. In our previous report, the average coefficient of thermal expansion of Nb-O bonds was -0.3322 10^{-6}/K and the temperature coefficient of resonant frequency was -21.96 ppm/°C for $Li_3Mg_2NbO_6$ ceramics [12]. In this paper, the average coefficient of thermal expansion of Nb-O bonds is -0.32778 10^{-6}/K and the temperature coefficient of resonant frequency is -15.45 ppm/°C for LNN ceramics. The temperature coefficient of resonant frequency shows the positive correlation with the coefficient of thermal expansion of Nb-O bonds for $Li_3Mg_2NbO_6$ and $Li_3Ni_2NbO_6$ ceramics.

It is known that the shorter bond length correlates with the higher bond energy, which indicates that the crystal would be more stable. The bond energy can be obtained through the chemical bond and electronegativity, which is reported by Sanderson [36, 37]. Based on the electronegativity and complex chemical bond theory, the formula for bond energy *E* can be written as Equs. (19-22).

$$E = \sum_{\mu} E_b^{\mu} \tag{19}$$

Where E_b^{μ} is the bond energy of the μ bond, which is composed by the nonpolar covalence energy E_c^{μ} and complete ionicity energy E_i^{μ} parts.

$$E_b^{\mu} = t_c E_c^{\mu} + t_i E_i^{\mu} \tag{20}$$

$$E_i^{\mu} = \frac{33200}{d^{\mu}} \tag{21}$$

For any binary compounds A_mB_n, the nonpolar covalence energy E_c^{μ} parts can be calculated as shown in Equ. 22.

$$E_c^{\mu} = \frac{(r_{cA} + r_{cB})}{d^{\mu}} (E_{A-A} E_{B-B})^{1/2} \tag{22}$$

Where r_{cA} and r_{cB} are the covalent radius, $E_{A\text{-}A}$ and $E_{B\text{-}B}$ are the homonucler bond energy. In this paper, $E_{Li\text{-}Li}$=105 kJ mol^{-1}, $E_{Ni\text{-}Ni}$=204 kJ mol^{-1}, $E_{Nb\text{-}Nb}$=513 kJ mol^{-1} and $E_{O\text{-}O}$=498.36 kJ mol^{-1}, which can be

obtained from the handbook [38]. The calculated results of the bond energy are listed in Table 4. According to the sequences of the average bond energy $AE_{(Ni-O)}<AE_{(Li-O)}<AE_{(Nb-O)}$, the bond energy $E_{(Nb-O)}$ makes the major influence to the τ_f for LNN ceramics. In our previous report, the average bond energy of Nb-O bonds was 586.0575 kJ mol^{-1} and the temperature coefficient of resonant frequency was -21.96 ppm/°C for $Li_3Mg_2NbO_6$ ceramics [12]. In this paper, the average bond energy of Nb-O bonds is 588.8015 kJ mol^{-1} and the temperature coefficient of resonant frequency is -15.45 ppm/°C for LNN ceramics. The temperature coefficient of resonant frequency shows the positive correlation with the bond energy of Nb-O bonds for $Li_3Mg_2NbO_6$ and $Li_3Ni_2NbO_6$ ceramics.

Fig. 7 shows the calculated and measured far infrared reflectivity spectra of LNN ceramics sintered at 850 °C. Based on the classical oscillator model, the complex dielectric function is written as Equ. 23 [39], and the complex reflectivity can be written as Equ. 24.

$$\varepsilon^*(\omega) = \varepsilon_\infty + \sum_{j=1}^{n} \frac{\omega_{pj}^2}{\omega_{oj}^2 - \omega^2 - j\gamma_j\omega} \tag{23}$$

$$R(\omega) = \left| \frac{1 - \sqrt{\omega^*(\omega)}}{1 + \sqrt{\omega^*(\omega)}} \right|^2 \tag{24}$$

where $\varepsilon^*(\omega)$ is the complex dielectric function, $R(\omega)$ is the complex reflectivity, n is the number of transverse phonon modes, ε_∞ is the dielectric constant caused by the electronic polarization, ω_{pj}, ω_{oj} and γ_j are the plasma frequency, transverse frequency and damping constant of the *J*-th Lorentz oscillator, respectively. As for LNN compounds, the space group has been introduced as Fddd (No. 70) and its point group is D2h (mmm). 40 infrared vibrational modes ($11B_{1u}+14B_{2u}+15B_{3u}$) are predicted for LNN compositions based on theoretical calculations. Twelve resonant modes can be detected and fitted for the measured infrared reflectivity spectrum as shown in Table 5. Some vibration modes are not detected because of their weak vibration characteristics. The calculated infrared reflectivity spectrum matches

well with the measured one, which can be observed in Fig. 7. In addition, the real (ε') and imaginary (ε'') parts of permittivity are plotted in Fig. 8. The extrapolated permittivity and dielectric loss from the fitted complex permittivity values (at around 11.85 GHz) of LNN are 7.2707 and 0.0003, respectively. It can be found that the calculated permittivity are smaller than the measured value and the calculated dielectric loss values are almost equal to the measured ones, which implies that the absorptions of phonon oscillation plays an important influence on the dielectric contribution of the LNN ceramics.

4. Conclusions

New LNN ceramics were successfully prepared by the solid-state method. The phase composition, crystal structure, sintering characteristics, micro-structures, microwave dielectric properties, intrinsic factors and vibrational phonon modes were investigated by XRD, SEM, FTIR, etc. XRD results showed that LNN phase exhibited orthorhombic structure with Fddd (No. 70) space group. The results of Infrared reflectivity spectrum implied that the absorptions of phonon oscillation played an important influence on the dielectric contribution of the LNN ceramics. LNN ceramics sintered at 850 °C can be well densified and reached a high relative density about 97.84 %. Based on the chemical bond theory and lattice parameters, the intrinsic parameters were calculated and microwave dielectric properties were strongly dependent on intrinsic factors. The dielectric constant could be strongly dependent on the bond ionicity of Nb-O bonds. The quality factor might be affected by the lattice energy of Nb-O bonds. The temperature coefficient of resonant frequency could be mainly influenced by the bond energy and coefficient of the thermal expansion of Nb-O bonds. Nb-O bonds played an important role in affecting the microwave dielectric proprieties of LNN ceramics. At the sintering temperature of 850 °C, LNN ceramics exhibited excellent microwave dielectric properties of ε_r=15.85, $Q \cdot f$=19,860 GHz and τ_f=-15.45 ppm/°C, which demonstrated that LNN ceramics were promising for the low temperature

co-fired ceramics applications.

Acknowledgments

This work was supported by the National Natural Science Foundation (No. 51472108). Authors are thankful to the administrators in IR beamline workstation of National Synchrotron Radiation Laboratory (NSRL) for the help in IR measurement.

References

1. A.N. Unnimaya, E.K. Suresh, R. Ratheesh, Mater. Res. Bull. 88 (2017) 174-181.

2. Z.F. Fu, J.L. Ma, P. Liu, B.C. Guo, X.M. Chen, Ceram. Int. 42 (2016) 6005-6009.

3. P. Zhang, J. Liu, Y.G. Zhao, H.Y. Du, X.Y. Wang, Mater. Lett. 162 (2016) 173-175.

4. J. Zhang, Y.Y. Zhou, Z.X. Yue, Ceram. Int. 39 (2013) 2051-2058.

5. H.T. Wu, E.S. Kim, RSC Adv. 6 (2016) 47443-47453.

6. S. Takahashi, A. Kan, H. Ogawa, J. Eur. Ceram. Soc. 37 (2017) 1001-1006.

7. J.J. Zhang, B. Shen, J.W. Zhai, X. Yao, Ceram. Int. 39 (2013) 5943-5948.

8. C.F. Xing, H.L. Pan, J.X. Bi, H.T. Wu, J Mater Sci: Mater Electron 27 (2016) 6558-6563.

9. H.D. Xie, H.H.Xi, F. Li, C. Chen, X.C. Wang, D. Zhou, J. Eur. Ceram. Soc. 34 (2014) 4089-4093.

10. J.X. Bi, Y.J. Niu, H.T. Wu, Ceram. Int. 43 (2017) 7522-7530.

11. L.L. Yuan, J.J. Bian, Ferroelectrics 387 (2009) 123-129.

12. H.T. Wu, E.S. Kim, J. Alloys Compd. 669 (2016) 134-140.

13. M. Castellanos, J.A. Gard, A.R. West, J. Appl. Cryst. 15 (1982) 116-119.

14. Y.G. Zhao, P. Zhang, J. Alloys Compd. 658 (2016) 744-748.

15. G.C. Mather, R.I. Smith, J.M.S. Skakle, J.G. Fletcher, M.A. Castellanos, M.P. Gutierrez, A.R. West, J. Mater. Chem. 5 (1995) 1177-1182.

16. G.C. Mather, A.R. West, J. Solid State Chem. 124 (1996) 214-219.

17. H. Kawasoko, R. Shimizu, Y. Takagi, K. Yamamoto, I. Sugiyama, S. Shiraki, T. Hitosugi, Thin Solid Films 621 (2017) 202-206.

18. B.W. Hakki, P.D. Coleman, IEEE Trans. 8 (1960) 402-410.

19. W.E. Courtney, IEEE Trans. 18 (1970) 476-485.

20. E.S. Kim, C.J. Jeon, P.G. Clem, J. Am. Ceram. Soc. 95 (2012) 2934-2938.

21. A. Thorvaldsen, Acta mater. 45 (1997) 595-600.

22. R.D. Shannon, G.R. Rossman, Am. Mineral. 77 (1992) 94-100.

23. R.D. Shannon, J. Appl. Phys. 73 (1993) 348-366.

24. J.C. Phillips, Phys. Rev. Lett. 20 (1968) 550-553.

25. J.C. Phillips, J.A. Van Vechten, Phys. Rev. Lett. 22 (1969) 705-708.

26. J.C. Phillips, Rev. Mod. Phys. 42 (1970) 317-356.

27. B.F. Levine, J. Chem. Phys. 59 (1973) 1463-1486.

28. B.F. Levine, Phys. Rev. B 7 (1973) 2591-2600.

29. D.F. Xue, S.Y. Zhang, J. Phys. Cond. Mat. 8 (1996) 1949-1956.

30. Z.J. Wu, Q.B. Meng, S.Y. Zhang, Phys. Rev. B 58 (1998) 958-962.

31. Q.B. Meng, Z.J. Wu, S.Y. Zhang, Phys. Cond. Mat. 10 (1998) 85-88.

32. Z.J. Wu, S.Y. Zhang, Int. J. Quantum Chem. 73 (1999) 433-437.

33. R.D. Shannon, Acta. Cryst. 32 (1976) 751-767.

34. A.F. Kapustinskii, Rev. Chem. Soc. 10 (1956) 283-294.

35. P. Zhang, Y.G. Zhao and Y.X. Wang, Dalton Trans. 44 (2015) 10932-10938.

36. R.T. Sandderson, Inorg. Nucl. Chem. 30 (1968) 375-393.

37. R.T. Sandderson, J. Am. Chem. Soc. 105 (1983) 2259-2261.

38. Y.R. Luo, Comprehensive Handbook of Chemical Bond Energies, CRC Press, Boca Raton 2007.

39. K. Wakino, M. Murata, H. Tamura, J. Am. Ceram. Soc. 69 (1986) 34-37.

Figures captions

Fig. 1 XRD diffraction patterns of $Li_3Ni_2NbO_6$ ceramics sintered at 750-950 °C

Fig. 2 A typical pattern plot of the $Li_3Ni_2NbO_6$ sample sintered at 850 °C after refinement all of the parameters (R_p=2.56 %, R_{wp}=3.26 % and χ^2=1.4)

Fig. 3 Schematic representation of the crystal structure for $Li_3Ni_2NbO_6$ ceramics

Fig. 4 Curves of the diametric shrinking ratio, apparent density and relative density of $Li_3Ni_2NbO_6$ samples as a function of sintering temperatures

Fig. 5 SEM micrographs of $Li_3Ni_2NbO_6$ ceramics sintered at different temperatures (a-e corresponding to 750 °C, 800 °C, 850 °C, 900 °C and 950 °C) and (f) EDS analysis about grains chosen randomly from the samples sintered at 850 °C.

Fig. 6 Curves of $\varepsilon_{r,}$ $Q{\cdot}f$ and τ_f values as a function of the sintering temperature from 750 °C to 950 °C

Fig. 7 Measured and fitted infrared reflectivity spectrum of $Li_3Ni_2NbO_6$ ceramics sintered at 850 °C

Fig. 8 Real and imaginary parts of complex permittivity for $Li_3Ni_2NbO_6$ ceramics

Table captions

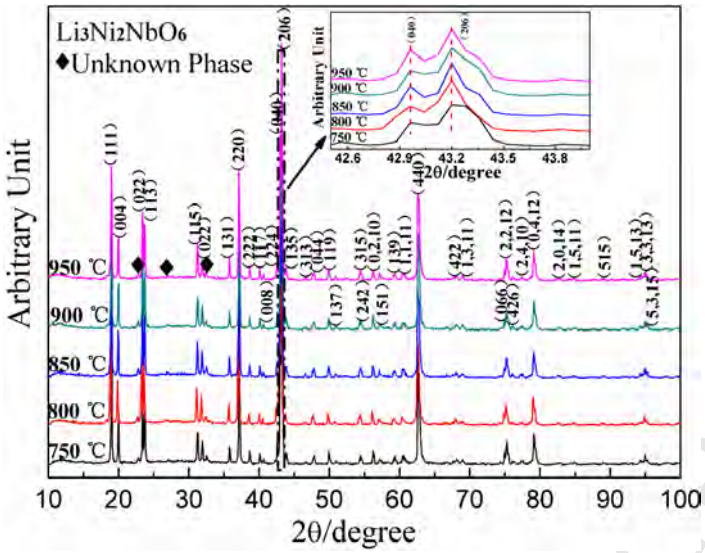

Fig. 1

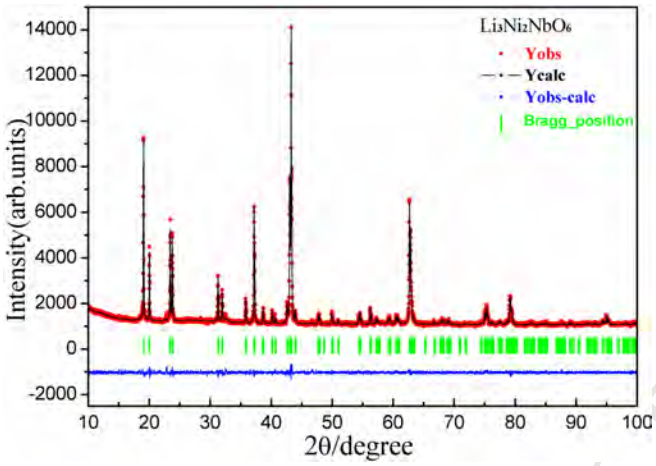

Fig. 2

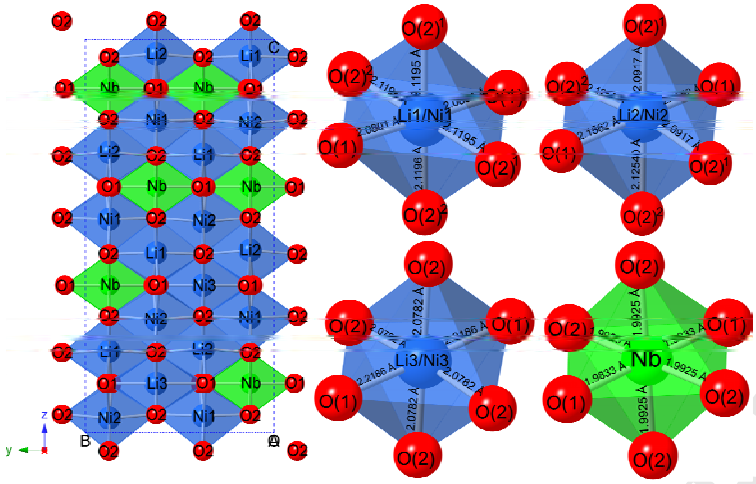

Fig. 3

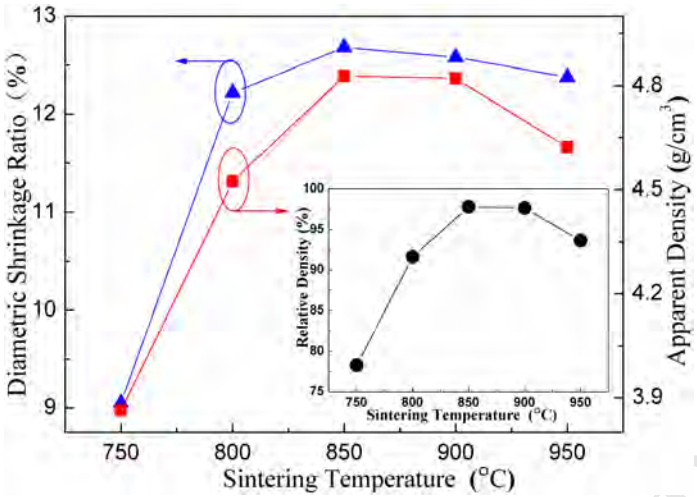

Fig. 4

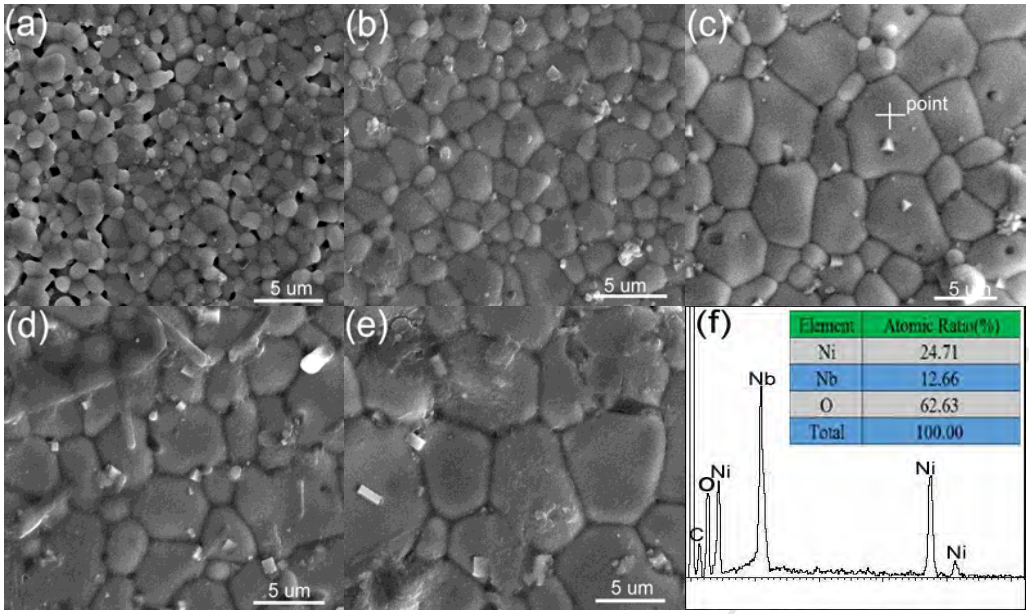

Fig. 5

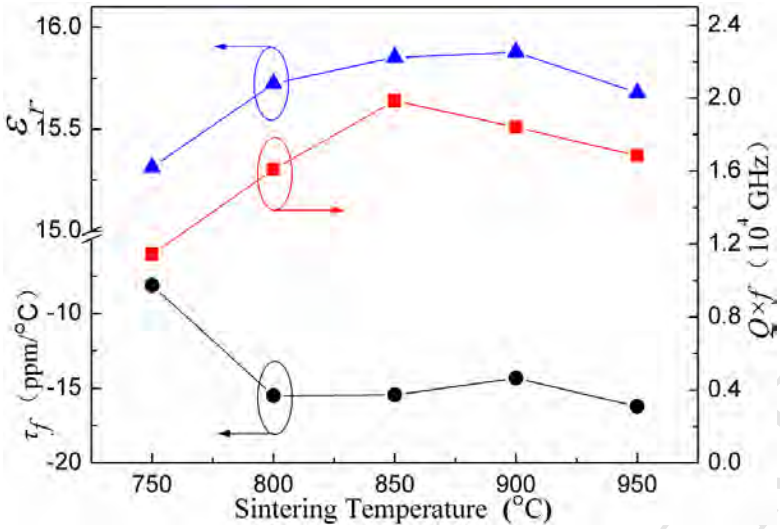

Fig. 6

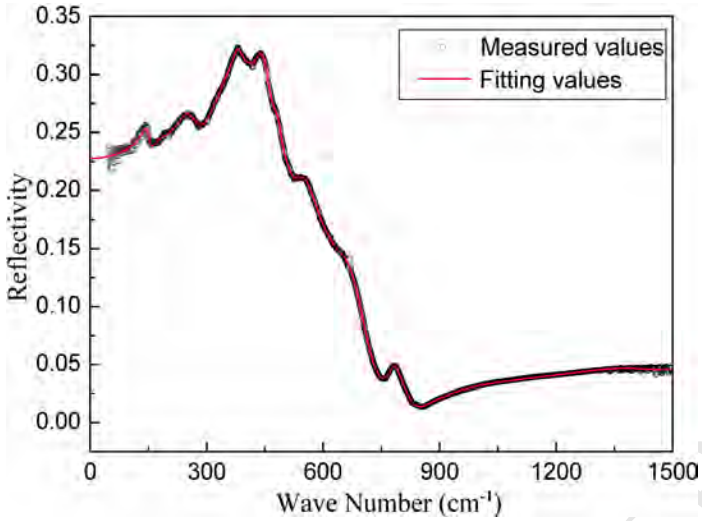

Fig. 7

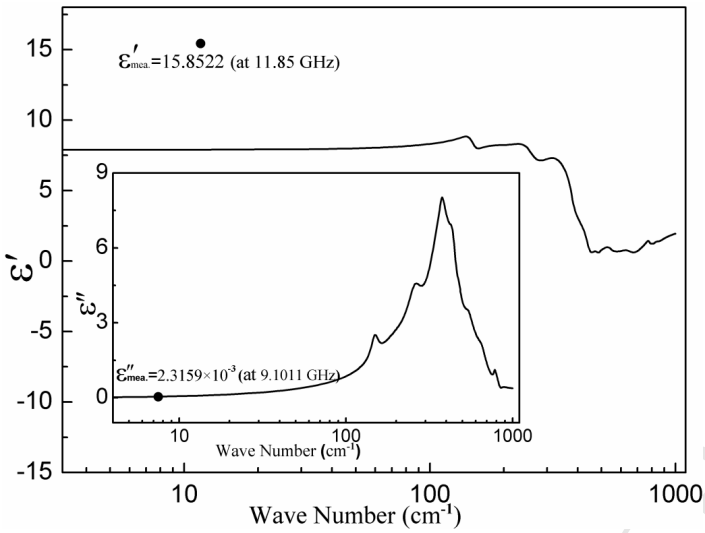

Fig. 8

Table 1

$Li_3Ni_2NbO_6$	Lattice parameters(Å)			Lattice parameters(°)			Vol(Å^3)
	a	b	c	α	β	γ	
	5.9066	8.4039	17.7444	90.0000	90.0000	90.0000	880.7927
Atom	x		y		z		Occupation
Li1	0.1250		0.1250		0.2919		0.3038
Ni1	0.1250		0.1250		0.2919		0.2156
Li2	0.1250		0.6250		0.2880		0.2494
Ni2	0.1250		0.6250		0.2880		0.2043
Li3	0.1250		0.6250		0.1250		0.1625
Ni3	0.1250		0.6250		0.1250		0.0875
Nb	0.1250		0.1250		0.1250		0.2500
O1	0.1250		0.3882		0.1250		0.5000
O2	0.1190		0.6912		0.4529		1.0000

Table 2

Atom1	Atom2	d1,2 [Å]	Atom1	Atom2	d1,2 [Å]
Nb1	O1	1.9833	Ni1|Li1	O1	2.0801
	O1	1.9833		O1	2.0801
	O2	1.9925		O2	2.1195
	O2	1.9925		O2	2.1195
	O2	1.9925		O2	2.1196
	O2	1.9925		O2	2.1196
Ni2|Li2	O1	2.1562	Ni3|Li3	O1	2.2186
	O1	2.1562		O1	2.2186
	O2	2.0917		O2	2.0782
	O2	2.0917		O2	2.0782
	O2	2.1254		O2	2.0782
	O2	2.1254		O2	2.0782

Table 3

Bond Type	Bond Length (Å)	f_i	f_c	U_{bc} (kJ/mol)	U_{bi} (kJ/mol)	U (kJ/mol)	$\alpha(10^{-6}K^{-1})$
Li1-O(1)×2	2.0801	95.7387	4.2613	17	661	678	7.4486
Li1-O(2)[1]×2	2.1195	95.7827	4.2173	17	652	669	7.5914
Li1-O(2)[2]×2	2.1196	95.7828	4.2172	17	652	669	7.5914
Li2-O(1)×2	2.1562	95.8210	4.1790	16	644	660	7.7382
Li2-O(2)[1]×2	2.0917	95.7520	4.2480	17	658	675	7.4958
Li2-O(2)[2]×2	2.1254	95.7890	4.2110	17	651	668	7.6075
Li3-O(1)×2	2.2186	95.8809	4.1191	16	630	646	7.9745
Li3-O(2)×4	2.0782	95.7365	4.2635	17	661	678	7.4486
Ni1-O(1)×2	2.0801	93.5871	6.4129	81	1292	1373	7.3171
Ni1-O(2)[1]×2	2.1195	93.6438	6.3562	79	1275	1354	7.4643
Ni1-O(2)[2]×2	2.1196	93.6440	6.3560	79	1275	1354	7.4643
Ni2-O(1)×2	2.1562	93.6931	6.3069	77	1259	1336	7.6075
Ni2-O(2)[1]×2	2.0917	93.6042	6.3958	80	1287	1367	7.3632
Ni2-O(2)[2]×2	2.1254	93.6520	6.3480	79	1272	1351	7.4879
Ni3-O(1)×2	2.2186	93.7695	6.2305	75	1232	1307	7.8466
Ni3-O(2)×4	2.0782	93.5842	6.4158	81	1293	1374	7.3095
Nb-O(1)×2	1.9833	98.7277	1.2723	75	12617	12692	-0.3327
Nb-O(2)×4	1.9925	98.7281	1.2719	74	12574	12648	-0.3228

Notes: (1) and (2) are used to distinguish oxygen atoms with different coordinate positions; [1] and [2] are used to distinguish oxygen atoms with different bond lengths.

Table 4

Bond Type	Bond Length (Å)	Ion coefficient	Covalent coefficient	E_c (kJ/mol)	E_i (kJ/mol)	E (kJ/mol)
Li1-O(1)×2	2.0801	0.4100	0.5900	215.5451	667.4794	400.8382
Li1-O(2)[1]×2	2.1195	0.4100	0.5900	211.5382	655.0715	393.3869
Li1-O(2)[2]×2	2.1196	0.4100	0.5900	211.5283	655.0406	393.3683
Li2-O(1)×2	2.1562	0.4100	0.5900	207.9377	643.9217	386.6912
Li2-O(2)[1]×2	2.0917	0.4100	0.5900	214.3497	663.7778	398.6152
Li2-O(2)[2]×2	2.1254	0.4100	0.5900	210.9510	653.2530	392.2948
Li3-O(1)×2	2.2186	0.4100	0.5900	202.0893	625.8109	375.8151
Li3-O(2)×4	2.0782	0.4100	0.5900	215.7421	668.0897	401.2046
Ni1-O(1)×2	2.0801	0.2533	0.7467	265.1848	667.4794	367.0994
Ni1-O(2)[1]×2	2.1195	0.2533	0.7467	260.2552	655.0715	360.2753
Ni1-O(2)[2]×2	2.1196	0.2533	0.7467	260.2429	655.0406	360.2583
Ni2-O(1)×2	2.1562	0.2533	0.7467	255.8254	643.9217	354.1432
Ni2-O(2)[1]×2	2.0917	0.2533	0.7467	263.7141	663.7778	365.0636
Ni2-O(2)[2]×2	2.1254	0.2533	0.7467	259.5327	653.2530	359.2752
Ni3-O(1)×2	2.2186	0.2533	0.7467	248.6301	625.8109	344.1826
Ni3-O(2)×4	2.0782	0.2533	0.7467	265.4272	668.0897	367.4350
Nb-O(1)×2	1.9833	0.3083	0.6917	539.3788	704.0575	590.1547
Nb-O(2)×4	1.9925	0.3083	0.6917	536.9068	700.8251	587.4483

Notes: (1) and (2) are used to distinguish oxygen atoms with different coordinate positions; [1] and [2] are used to distinguish oxygen atoms with different bond lengths.

Table 5

Modes	ε_∞=2.2685			
	ω_{oj}	ω_{pj}	γ_j	$\Delta_{\varepsilon j}$
1	149.0772	49.3578	18.0775	0.1100
2	207.5350	185.5221	145.1865	0.7990
3	260.0397	164.7508	63.6719	0.4010
4	377.6202	88.6457	30.0673	0.0551
5	385.1411	632.2428	164.1304	2.6900
6	437.1054	184.9732	50.2128	0.1790
7	478.3882	70.3179	28.2786	0.0216
8	545.5780	56.4724	35.4501	0.0107
9	553.5529	407.1881	175.4439	0.5410
10	655.1220	240.4489	113.4604	0.1350
11	782.1799	83.9420	27.4507	0.0115
12	802.0121	81.8914	38.7496	0.0483

Research highlights

- New low-temperature sintering $Li_3Ni_2NbO_6$ ceramics were prepared.
- Rietveld refinement was used and lattice parameters were obtained.
- Bond ionicity, lattice energy and bond energy were caluclated.
- Infrared reflectivity spectrum was used to analyze the vibrational phonon modes.